

The studies on phonons and magnons in (Ni₈₀Fe₂₀/Au/Co/Au) multilayers of different number of repetitions

M. Zdunek^{1*}, A. Trzaskowska¹, J. W. Kłos¹, N.K.P. Babu¹, S. Mielcarek¹

¹ Faculty of Physics, Adam Mickiewicz University in Poznań, Poznań, Poland

* E-mail: milosz.zdunek@amu.edu.pl

Abstract

In Ni₈₀Fe₂₀/Au/Co/Au deposited on silicon substrate the interaction between spin waves and surface acoustic waves is observed by Brillouin light scattering spectroscopy. We show that by changing the number of receptions in the multilayer we can tune the dispersion of surface acoustic waves (SAWs) not affecting significantly fundamentals spin wave (SW) mode. As a result, we can control (activate or deactivate) the magnetoelastic interaction between fundamental SW mode and SAWs by the thickness of the magnetostrictive multilayer.

Keywords: surface acoustic waves, spin waves, Brillouin light scattering spectroscopy, finite element method

1. Introduction

The magnetic nanostructures have promising applications in magnonic where the spin waves (SWs) are used to transmit and process information [1,2]. The functionality of magnonics devices can be also tailored and controlled by elastic properties and elastic excitations [3-15]. The particularly interesting is considering the impact of elastic waves on spin waves. However, this approach requires the appropriate selection of elastic and magnetic properties of the system

to observe the phononic and magnonic dispersion branches in the same ranges of frequency and wave vector [16-18]. The (anticrossing) of magnonic and phononic dispersion branches is a necessary condition for magnetoelastic coupling between SWs and elastic waves. It expresses the conservation of momentum and energy for the elastic scattering of interacting quasiparticles: magnon and phonon.

The ferromagnetic layer deposited on elastic and nonmagnetic substrate enables the simultaneous propagation of surface acoustic waves (SAWs) as well as SWs [3-7]. This is a simple structure that seems to be a basic magnonic-phononic hybrid system. However, the dispersion branches of SAWs are observed at relatively low frequencies, significantly below the ferromagnetic resonance (FMR) frequencies of the film, made of typical magnonics materials of low damping (Py, CoFeB) and placed in relatively low, in-plane applied, magnetic fields (few tens of mT).

To overcome this problem, we can replace the magnetic layer with a multilayer, where thin magnetic and non-magnetic layers are interleaved. For the fundamental SW mode and the lowest perpendicularly standing SW modes, the multilayer is perceived as a homogeneous material of lowered effective saturation magnetization which reduces the frequencies of magnonics dispersion branches, allowing for interaction with SAWs [16-18]. The coupling between SW and SAW is weak, therefore the (anti)crossings of the magnonic and phononic dispersion branches should be carefully analyzed. Moreover, the magnetoelastic interaction depends on the orientation of the wave vector, concerning the direction of the static magnetic field, and the spatial profiles of SAWs [8,18-19]. These dependencies are specific for particular kinds of SAWs.

In our work, we are discussing the magnonics and phononic properties of (Ni₈₀Fe₂₀/Au/Co/Au) multilayers deposited on the silicon substrate. In the considered system, the permalloy layers (of low saturation magnetization) are magnetized in-plane, whereas the

very thin cobalt layers (of high saturation magnetization) are magnetized out-of-plane due to the magnetocrystalline anisotropy. The cobalt subsystem is weakly excited by SWs for the frequency range where we observe SAWs. We intended to use the cobalt layers as sources of the stray field which acts on SW dynamics in permalloy equivalently to perpendicular anisotropy. Such anisotropy lowers the FMR frequency for in-plane magnetized films [20]. This effect, complementary to the reduction of effective magnetization [18], and can be used to tailor the SW spectra for the observation of the interaction with SAWs. The number of receptions of Co, Py, Au layers with the multilayer does not change the FMR frequency but will certainly affect the frequencies of SAW. Our main goal is to study the impact of the number of repetitions in the (Ni₈₀Fe₂₀/Au/Co/Au) multilayer on SAW dispersion and then on the magnetoelastic interaction with SW. We present the results of Brillouin light scattering (BLS) measurements and finite element methods (FEM) calculations to determine and analyze magnonic and phononic dispersion relation in this system.

2. Materials and methods

2.1. The samples

The studied multilayer [Ni₈₀Fe₂₀/Au/Co/Au]_N is composed of number of repetition (N) of permalloy (of the thickness $t_{\text{NiFe}}=2$ nm) and cobalt layers ($t_{\text{Co}}=0.8$ nm), sandwiched with gold layers ($t_{\text{Au}}=2$ nm). The multilayer was deposited on the gold buffer ($t_{\text{BAu}}=35$ nm). The substrate for the investigated sample was naturally oxidized (100) silicon. The layers were deposited in an argon atmosphere using high vacuum magnetron sputtering on the substrate [21]. The magnetic field $\mu_0 H=50$ mT has been applied in the plane of the sample. A schematic sketch of the sample and scattering geometry has been shown in Fig. 1.

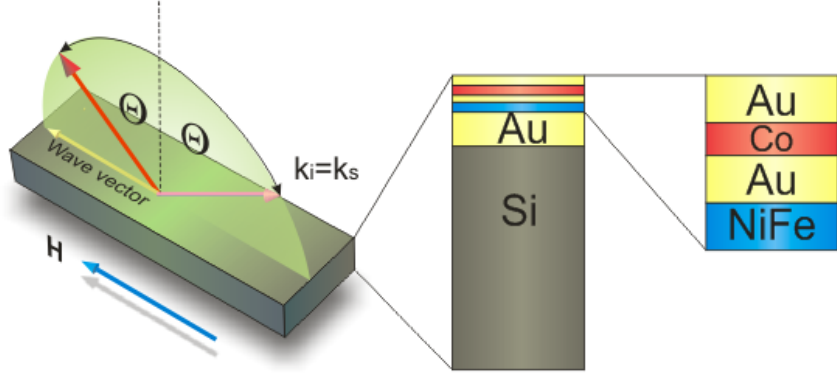


Fig. 1. Schematic sketch of the considered system, composed of thick silicon (100) substrate with the gold buffer layer and magnetic multilayer. At the surface of the substrate loaded by the multilayer, the surface acoustic waves (SAWs) can propagate. The spin waves (SWs) of long-wavelength can propagate in a magnetic multilayer structure. The magnetic field H (blue arrow) is applied in the plane of the sample and is parallel to the plane of incidence for the light (photons) which interacts with magnons and phonons (red arrows denote the wave vectors k_i, k_s for incidence and scattered light). Permalloy (NiFe) layers are magnetized in-plane, whereas cobalt (Co) layers – out-of-plane, due to the strong magnetocrystalline anisotropy of Co. The wavevector for SAWs and SWs (yellow arrow) has the same direction as the applied field (backward volume geometry for SWs in NiFe).

2.2. Experimental setup

To obtain the dispersion relations of SAWs and SWs, we used a six-pass, tandem Brillouin spectrometer (TFP2-HC, JRS) which ensures a contrast of 10^{15} [22]. The source of scattering light was a frequency stabilized DPSS laser, which operates at $\lambda_0 = 532$ nm (Coherent Verdi V5). The geometry used for those measurements was a 180° backscattering geometry with pp polarization for SAWs and ps polarization for SWs. The frequency of SAWs and SWs is represented by the Brillouin frequency shift of the inelastically scattered laser beam. Changing the angle of light incidence, Θ , concerning the surface of the sample, allows selecting the wave vector ($q = \frac{4 \cdot \pi \cdot \sin(\Theta)}{\lambda_0}$), common for SAWs and SWs, and determining the dispersion relation

[23-25]. In our experiments, the wave vector was varied in the range 0.007-0.022 nm⁻¹ with a resolution of about 0.004 nm⁻¹. The free spectral range (FSR) was 20 GHz with a frequency resolution of about 0.04 GHz. The sample was placed in the external magnetic field (50 mT), aligned with the wave vector, which corresponds to backward volume (BV) geometry for SWs in permalloy. Each spectrum was accumulated for 6000 cycles. A Lorentzian curve was fitted for each peak. A more detailed description of the experimental setup can be found in [26].

2.3. FEM simulations

The dispersion relation for SAWs propagating in the studied sample was simulated using the finite element method code of COMSOL Multiphysics with Acoustic module [27]. The multilayers structure had been treated as one uniform material with elastic constant: $c_{11}=c_{22}=c_{33}=213.6\times 10^9$ N/m², $c_{44}=c_{55}=c_{66}=44.7\times 10^9$ N/m², $c_{12}=c_{13}=c_{23}=124.1\times 10^9$ N/m² and mass density $\rho = 14948$ kg/m³. The main components of the elasticity tensor for buffer gold layer was: $c_{11}=c_{22}=c_{33}=192.3\times 10^9$ N/m², $c_{44}=c_{55}=c_{66}=41.9\times 10^9$ N/m², $c_{12}=c_{13}=c_{23}=163.1\times 10^9$ N/m², and density $\rho = 19300$ kg/m³ while for silicon substrate it was: $c_{11}=c_{22}=c_{33}=166.6\times 10^9$ N/m², $c_{44}=c_{55}=c_{66}=79.6\times 10^9$ N/m², $c_{12}=c_{13}=c_{23}=64\times 10^9$ N/m² and mass density $\rho = 2331$ kg/m³ [28, 29]. The elastic constants and the mass densities of each material take into account the crystallographic orientation. The idea of calculating the dispersion relation for phononic samples was presented in Ref. [30-32].

4. Results

The larger number of repetitions N in the multilayer [NiFe/Au/Co/Au]_N, means the increase of total thickness of the multilayer which affects significantly the spectrum of SAWs. The spectra obtained for the samples with repetition $N=3$ and 12 of a [Ni₈₀Fe₂₀/Au/Co/Au]_N multilayer are presented in Fig. 2.

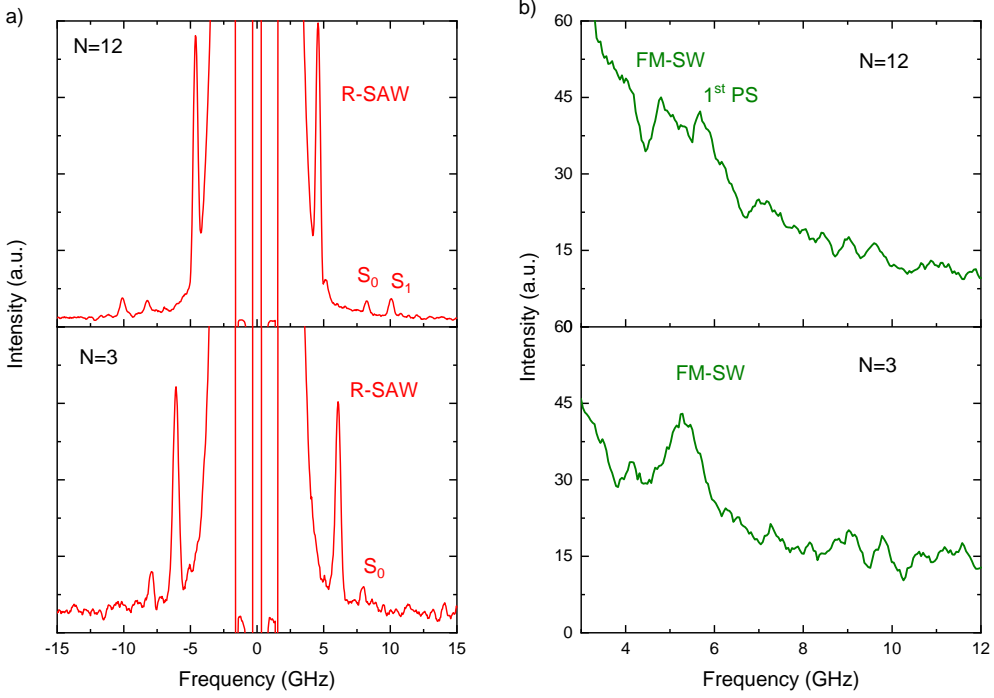


Fig. 2. (a) The BLS spectra for phonons depending on the number of repetitions $[\text{Ni}_{80}\text{Fe}_{20}/\text{Au}/\text{Co}/\text{Au}]_N$ for the wave vector $q=0.01692 \text{ nm}^{-1}$ with visible Rayleigh SAW (R-SAW) and Sezawa SAW (S_0, S_1). (b) Spin wave BLS spectra for $[\text{Ni}_{80}\text{Fe}_{20}/\text{Au}/\text{Co}/\text{Au}]_N$ multilayers differing in the number of receptions N . The spectra were measured for the geometry supporting BV modes (in-plane field perpendicular to wave vector) at the field 50 mT and wave vector 0.01360 nm^{-1} . For thicker samples ($N=12$), we see two distinctive peaks which can be attributed to the fundamental mode (FM) and first perpendicularly standing mode (1st PS). For a thinner sample, we can see the only fundamental mode of almost the same frequency – perpendicularly standing SW modes were pushed up in frequency scale and are not detected in this spectrum.

The SAW with the smallest frequency corresponds to the Rayleigh surface acoustic wave (R-SAW). This kind of wave can be observed in all solid-state materials. Other modes, which are visible in the spectra, are the Sezawa surface acoustic modes (S_0-S_1). The number of the Sezawa SAWs, observed in a fixed frequency range, is larger for thicker multilayers (i.e. for multilayers of a larger number of repetitions N). Sezawa SAWs are typical for the overlayer-substrate system [31]. By considering the values of elastic properties for the

substrate, and complex overlayer (buffer layer and multilayers), the studied structure can be classified as a so-called *slow-on-fast* system [26, 31]. This feature can be confirmed by analyzing the dependence of the phase velocity of SAWs v on the wave vector q .

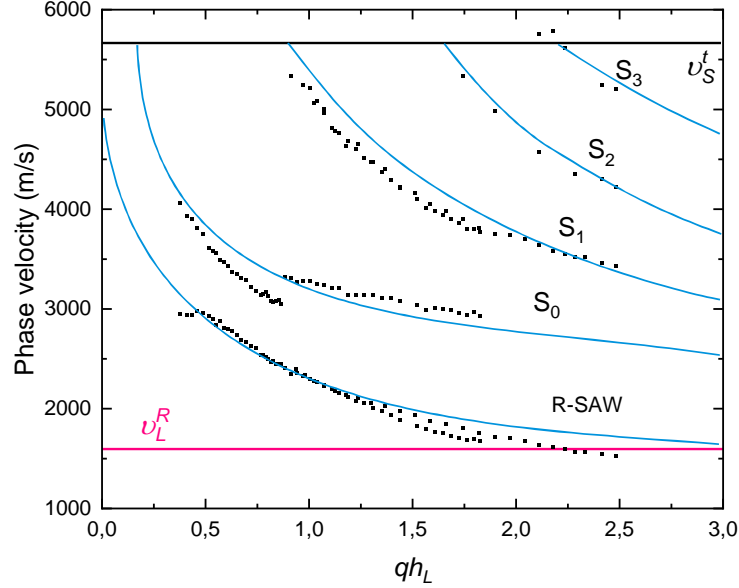


Fig. 3. The phase velocity v of SAWs in dependence on dimensionless wave number qh_L , where $h_L=N(t_{\text{Au}}+t_{\text{NiFe}}+t_{\text{Au}}+t_{\text{Co}})+t_{\text{BAu}}$ stands for the thickness of the complex overlayer. The points and lines correspond to experimental and numerical outcomes for R-SAW and Sezawa SAWs (S_0 - S_3). Please note that the experimental data were aggregated from all investigated samples, differing in the number of repetitions N . The horizontal lines v_L^R v_S^t mark the phase velocities for overlayer (isolated from the substrate) and substrate (unloaded), respectively.

With the increase of the wave vector, the SAWs become more localized. They penetrate the substrate weaker and are stronger concentrated in the overlayer. For large values of qh_L the phase velocity approaches the value for isolated overlayer v_L^R . On the other hand, in the limit $qh_L=0$ the occupation of overlayer by SAW is negligible comparing to the substrate and the limiting phase velocity corresponds to the velocity of bare substrate v_S^R . The negative slopes for all SAWs, visible in Fig.3, are consistent with the conditions $v_S^t > v_L^t$ for the *slow-on-fast* system. The numerical results, presented in Fig.3, were obtained by FEM calculations

described in Ref.28 whereas the experimental outcomes originate from the BLS measurements (phase velocity is a ratio of frequency and wave vector).

The magnetic properties of the $[\text{Ni}_{80}\text{Fe}_{20}/\text{Au}/\text{Co}/\text{Au}]_N$ multilayers are particularly interesting. The cobalt layer in such structures has out-of-plane oriented magnetization as opposed to a layer of permalloy for which the magnetization is oriented in-plane. The SW eigenmodes of the lowest frequencies will be predominately concentrated in NiFe characterized by lower saturation magnetization and FMR frequency. The cobalt subsystem is supposed to serve as a source of a static stray field which can be equivalent to the presence of the perpendicular anisotropy for in-plane magnetized permalloy layers.

The obtained dispersion relations of SAWs and SWs (for the configurations supporting BV modes) have been shown in Fig.4. We showed the dispersion relation in a selected range of the wave vector to observe the area of anticrossing of the phononic and SW dispersion curves. Fig.4 present the results for the structures differing in the number of repetitions within the $[\text{Ni}_{80}\text{Fe}_{20}/\text{Au}/\text{Co}/\text{Au}]_N$ multilayers: $N=3$ in Fig.4a and $N=12$ in Fig.4b.

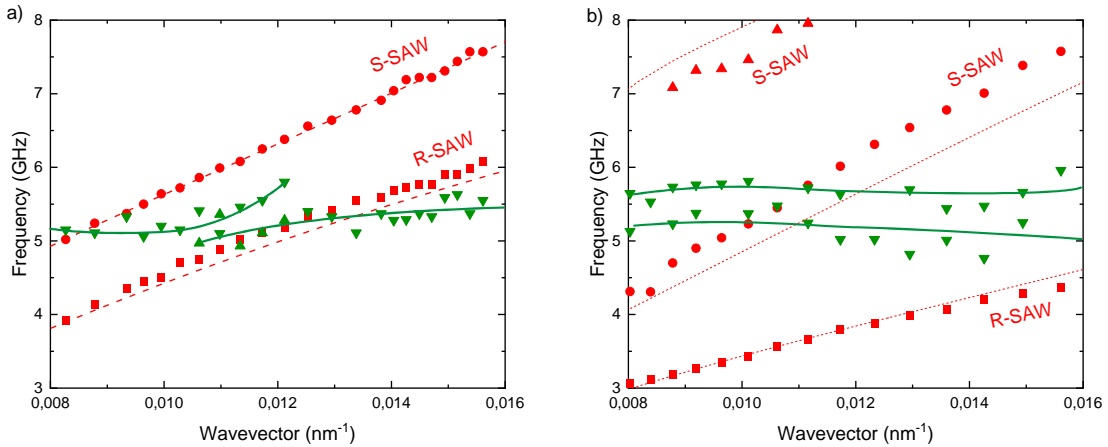


Fig. 4. Dispersion relations measured for SAWs (red points) and SWs (green points) for the BV geometry in structure with $N=3$ (a) and $N=12$ (b) repetitions in the $[\text{Ni}_{80}\text{Fe}_{20}/\text{Au}/\text{Co}/\text{Au}]_N$ multilayer. The red dashed line shows the calculated dispersion relations for R-SAW and lowest Sezawa SAW (S-SAW). (a) The continuous green line is drawn, as a guide for the eye, to show the expected dispersion

of hybridized (anticrossed) SW fundamental mode (SW-F) and Love SAW (see Ref. 18). (b) The continuous green line is drawn, as a guide for the eye, to show the expected dispersion fundamental SW (F-SW) mode and the first perpendicular standing SW (1st PS-SW) mode.

The increase of the thickness of the overlayer (due to the larger number of receptions N in the $[\text{Ni}_{80}\text{Fe}_{20}/\text{Au}/\text{Co}/\text{Au}]_N$ multilayer), results in the significant decrease of the phase velocity (and group velocity) for SAWs which is observed as a reduction of the slope of SAW dispersion branches in Fig.4. The F-SW mode is quite robust on the changes of the thickness of the magnetostrictive multilayer whereas the PS-SW modes are shifted down in frequency scale due to weaker confinement in the multilayer.

In the considered geometry, supporting the BV SW, the magnetoelastic interaction between SWs and R-SAWs (or S-SAWs) is extremely weak [6,18]. The interaction can be observed for F-SW mode and Love SAW [18]. However, the Love SAW is barely detectable in the BLS measurements. In our studies, the Love SAW is visible only due to its hybridization with F-SW mode visible in Fig.4a. In the numerical studies, we used the simplified model where only the displacements characteristic for R-SAWs and S-SAWs were taken into account and the magnetoelastic coupling was excluded. By referring to the previous work [18], we attributed the anticrossing visible at F-SW mode to the interaction with Love SAW. We showed that this interaction can be tailored by the change of thickness for a magnetostrictive layer which leads to the adjustment of the slope of the dispersion branches for SAWs, and does not affect noticeably on F-SW mode.

The interaction between SAWs and SWs was possible to observe because we were able to design the magnetostrictive multilayer of reduced saturation magnetization (due to the presence of non-magnetic component – Au) and with an induced static out-of-plane field (produced by cobalt layers), acting equivalently to perpendicular anisotropy. It is worth to note that the FMR frequency (i.e. the frequency of F-SW mode at $q=0$) can be estimated from the formula [33]:

$$f_{FMR} = \frac{\mu_0 \gamma}{2\pi} \sqrt{H(H - H_a + M_S)}, \quad (1)$$

where $M_S = 550$ kA/m is effective saturation magnetization, calculated as a volume average of the constituent materials of the multilayer (i.e. for 1300 kA/m for Co and 800 kA/m for NiFe), and H_a is perpendicular anisotropy field (i.e. the stray field produced by Co layers). The expression $\gamma/2\pi=28.02$ GHz/T is a gyromagnetic ratio. By assuming $H_a = 0$, we obtain slightly overestimated values of $f_{FMR}=5.35$ GHz. Therefore, it is required to take some non-zero value of H_a .

6. Conclusions

The experimental results show the interaction between spin waves and surface acoustic waves in magnetic multilayer $[\text{Ni}_{80}\text{Fe}_{20}/\text{Au}/\text{Co}/\text{Au}]_N$ deposited on a silicon substrate with Au buffer layer. The number of repetitions N within the multilayer affects the phase velocity of surface acoustic waves and does not influence significantly the fundamental mode for backward volume spin waves. Therefore, the interaction between both kinds of waves can be adjusted only by the change of the dispersion of surface acoustic waves resulting from the tuning of the thickness of the multilayer.

We suppose that for the eigenfrequencies below the FMR frequency for cobalt, the magnetization dynamics in the $[\text{Ni}_{80}\text{Fe}_{20}/\text{Au}/\text{Co}/\text{Au}]_N$ multilayer is focussed in permalloy. Moreover, the perpendicularly magnetized cobalt layers provide the out-of-plane stay field which acts similarly to the perpendicular anisotropy and reduces the FMR frequency for in-plane magnetized permalloy layers.

Acknowledgement:

This work was supported by Polish National Science Centre under grant no. UMO-2016/21/B/ST3/00452 and the EU's Horizon 2020 Research and Innovation Program under Marie Skłodowska –Curie Grant Agreement No. 644348 (MagIC).

References

- [1] A. Chumak, V. Vasyuchka, A. Serga, B. Hillebrands, Magnon spintronics, *Nature Phys.* 11, (2015) 453 . DOI: 10.1038/NPHYS3347
- [2] M. Krawczyk, D. Grundler, Review and prospects of magnonic crystals and devices with reprogrammable band structure, *J. Phys.: Condens. Matter* 26, (2014) 123202 (32pp). doi:10.1088/0953-8984/26/12/123202
- [3] M. Weiler, H. Huebl, F.S. Goerg, F.D. Czeschka, R. Gross, S.T.B. Goennenwein, Spin pumping with coherent elastic waves, *Phys. Rev. Lett.* 108 (2012) 176601, <https://doi.org/10.1103/PhysRevLett.108.176601>.
- [4] K. An, et al., Magnons and Phonons Optically Driven Out of Local Equilibrium in a Magnetic Insulator, *Phys. Rev. Lett.* 117 (2016) 107202, doi.org/10.1103/PhysRevLett.117.107202.
- [5] S.L. Holm, A. Kreisel, T.K. Schaffer, A. Bakke, M. Bertelsen, U.B. Hansen, M. Retuerto, J. Larsen, D. Prabhakaran, P.P. Deen, Z. Yamani, J.O. Birk, U. Stuhr, Ch. Niedemayer, A.L. Fennell, B.M. Andersen, K. Lefmann, Magnetic ground state and magnon-phonon interaction in multiferroic h-YMn₃, *Phys. Rev. B* 97 (2018) 134304, <https://doi.org/10.1103/PhysRevB.97.134304>.
- [6] J. Holanda, D.S. Maior, A. Azevedo, S.M. Rezende, Detecting the phonon spin in magnon–phonon conversion experiments, *Nat. Phys.* 14 (2018) 500–506, <https://doi.org/10.1038/s41567-018-0079-y>.
- [7] C. Berk, M. Jaris, W. Yang, S. Dhuey, S. Cabrini, H. Schmidt, Strongly coupled magnon–phonon dynamics in a single nanomagnet, *Nat. Comm.* 10 (2019) 2652, <https://doi.org/10.1038/s41467-019-10545-x>.
- [8] L. Dreher, et al. Surface acoustic wave driven ferromagnetic resonance in nickel thin films: Theory and experiment, *Phys. Rev. B* 86 (2012) 134415, <https://doi.org/10.1103/PhysRevB.86.134415>.
- [9] P. Graczyk, J.W. Kłos, M. Krawczyk, Broadband magnetoelastic coupling in magnonic-phononic crystals for high-frequency nanoscale spin-wave generation, *Phys. Rev. B* 95 (2017) 104425, <https://doi.org/10.1103/PhysRevB.95.104425>.

[10] K. An, et al., Coherent long-range transfer of angular momentum between magnon Kittel modes by phonons, *Phys. Rev. B* 101, (2020) 060407 (R). 10.1103/PhysRevB.101.060407

[11] S. Streib, N. Vidal-Silva, K. Shen, G.E.W. Bauer, Magnon-phonon interactions in magnetic insulators, *Phys. Rev. B* 99, (2019) 184442. <https://doi.org/10.1103/PhysRevB.99.184442>

[12] A. Kamra, H. Keshtgar, F. Yan, G. Bauer Coherent elastic excitation of spin waves, *Phys. Rev. B* 91, (2015) 104409 . DOI: 10.1103/PhysRevB.91.104409

[13] J. Cramer, et al., Magnon detection using a ferroic collinear multilayer spin valve, *Nat. comm.* 9, (2018) 1089. DOI: 10.1038/s41467-018-03485-5

[14] D. Bozhko, V. Vasyuchka, A. Chumak, A. Serga, Magnon-phonon interactions in magnon spintronics, *Low Temp. Phys.* 46, (2020) 383. <https://doi.org/10.1063/10.0000872>

[15] D. Lachance-Quirion, Y. Tabuchi, A. Gloppe, K. Usami, Y. Nakamura, Hybrid quantum systems based on magnonics. *Appl. Phys. Express* 2019, 12, 070101.

[16] N.K.P. Babu, A. Trzaskowska, S. Mielcarek, H. Głowinski, O. M. Chumak, M. Zdunek, J. W. Kłos, M. Krawczyk, Interaction Between Thermal Magnons and Phonons in a CoFeB/Au Multilayer. *IEEE Magn. Lett.* 2019, 10, 1–5.

[17] M. Zdunek, A. Trzaskowska, J. W. Kłos, N. K. P. Babu, S. Mielcarek, Investigation of phonons and magnons in $[Ni_{80}Fe_{20}/Au/Co/Au]_{10}$ multilayers. *J. Magn. Magn. Mater.* 2020, 500, 166428

[18] N. K. P. Babu, A. Trzaskowska, P. Graczyk, G. Centała, S. Miesczak, H. Głowiński, M. Zdunek, S. Mielcarek, and J. W. Kłos, The interaction between surface acoustic waves and spin waves – the role of anisotropy and spatial profiles of the modes, *Nanoletters* (2020), <https://dx.doi.org/10.1021/acs.nanolett.0c03692>

[19] C. L. Chang, S. Miesczak, M. Zelent, V. Besse, U. Martens, R.R. Tamming, J. Janusonis, P. Graczyk, M. Münzenberg, J.W. Kłos, and R. I. Tobey, Driving Magnetization Dynamics in an On-Demand Magnonic Crystal via the Magnetoelastic Interactions, *Phys. Rev. Applied* 10, 064051 (2018).

[20] A. Gurevich, G. Melkov, *Magnetization Oscillations and Waves*; CRC, Boca Raton, (1996).

[21] M. Urbaniak, F. Stobiecki, B. Szymański, A. Ehresmann, A. Maziewski, M.J. Tekielak, 2007. Magnetic and magnetoresistive properties of NiFe/Au/Co/Au multilayers with perpendicular anisotropy of Co layers. *J. Appl. Phys.* 101, 013905. <https://doi.org/10.1063/1.2403972>.

[22] F. Scarponi, S. Mattana, S. Corezzi, S. Caponi, L. Comez, P. Sassi, A. Morresi, M. Poalantoni, L. Urbanelli, C. Emiliani, L. Roscini, L. Corte, G. Cardinali, F. Palombo, J.R. Sandercock, D. Fioretto, High-Performance Versatile Setup for Simultaneous Brillouin-Raman Microspectroscopy, *Phys. Rev. X* 7 (2017) 031015, <https://doi.org/10.1103/PhysRevX.7.031015>.

[23] H. Pan, V.L. Zhang, K. Di, M.H. Kuok, H.S. Lim, S.C. Ng, N. Singh, A.O. Adeyeye, Phononic and magnonic dispersions of surface waves on a permalloy/BARC nanostructured array, *Nanoscale Res. Lett.* 8 (2013) 115, <https://doi.org/10.1186/1556-276X-8-115>.

[24] G. Gubbiotti, R. Silvani, S. Tacchi, M. Madami, G. Carlotti, Z. Yang, A.O. Adeyeye, M. Kostylev, Tailoring the spin waves band structure of 1D magnonic crystals consisting of L-shaped iron/permalloy nanowires, *J. Phys. D: Appl. Phys.* 50 (2017), <https://doi.org/10.1088/1361-6463/aa59a4>.

[25] C.E. Bottani, D. Fioretto, Brillouin scattering of phonons in complex materials, *Adv. Phys.: X* 3 (1) (2018) 1467281, <https://doi.org/10.1080/23746149.2018.1467281>.

[26] A. Trzaskowska, S. Mielcarek, B. Graczykowski, B. Mroz, P. Patoka, M. Giersig, The effect of nickel nanostructure on surface waves propagation in silicon support, *J. Alloys Compd.* 527 (2012) 96. <https://doi.org/10.1016/j.jallcom.2012.03>.

[27] COMSOL Multiphysics finite element software, COMSOLAB, Sweden.

[28] G.W. Farnell, E.L. Adler, Elastic wave propagation in thin layers in *Physical Acoustics* 9 (Academic Press, New York, 1972) p. 35. <https://doi.org/10.1016/B978-0-12-395670-5.50007-6>.

[29] J.R. Neighbours, G.A. Alers, Elastic constant of silver and gold, *Phys. Rev.* 111 (1958) 707–712. <https://doi.org/10.1103/PhysRev.111.707>

[30] A. Trzaskowska, S. Mielcarek, B. Graczykowski, F. Stobiecki, Surface waves investigation in NiFe/Au/Co/Au multilayers by high-resolution Brillouin spectroscopy, *J. Alloys Comp.* 517 (2012) 132–138. <https://doi.org/10.1016/j.jallcom.2011.12.059>.

[31] G.W. Farnell, Properties of elastic surface waves in *Physical Acoustics* 6 (Academic Press, New York, 1970) p. 109–166. <https://doi.org/10.1016/B978-0-12-395666-8.50017-8>

[32] A. Trzaskowska, S. Mielcarek, J. Sarkar, 2013. Band gap in hypersonic surface phononic lattice of nickel pillars. *J. Appl. Phys.* 114 134304. <https://doi.org/10.1063/1.4824103>.

[33] T. Kundu, *Ultrasonic Nondestructive Evaluation Engineering and Biological Material Characterization* CRC Press, (2003).

